THE EXISTENCE OF LONG-LIVED RAYS OF THE CORONAL STREAMER BELT – RADIAL DENSITY AND VELOCITY DISTRIBUTIONS OF THE SOLAR WIND FLOWING IN THEM

V. G. ESELEVICH, V. G. FAINSHTEIN and M. V. ESELEVICH
Institute of Solar-Terrestrial Physics, P.O. Box 4026, 664033 Irkutsk, Russia
(e-mail: esel@iszf.irk.ru)

(Received 25 August 2000; accepted 22 December 2000)

Abstract. A technique is proposed for separating the rays of the streamer belt with quasi-stationary and non-stationary solar wind (SW) flows. It is shown that the lifetime of rays with a quasi-stationary SW can exceed 20 days. A new method has been developed for measuring the relative density distribution of a quasi-stationary slow SW flowing along the streamer belt's ray of increased brightness, based on the LASCO/SOHO data. It is shown that the density n for such SW flows varies with the radius R according to the relationship $n \sim R^{-\alpha}$, where $\alpha = \alpha_1 \approx 3.3$–$3.9$ within $4\ R_0 \leq R \leq 6\ R_0$ (here R_0 is the solar radius), and decreases gradually further away. It is also shown that the $V(R)$-profiles in some rays of the streamer belt differ little from each other, although the value of the mass flow density, j_E, at the Earth's orbit in them can vary more than by a factor of 4. This distinguishes in a crucial respect a slow SW in the streamer belt's rays from a fast SW originating in coronal holes, for which $j_E \approx$ constant and the dependences $V(R)$ in different fast flows can differ greatly.

1. Introduction

According to current concepts, the coronal streamer belt is the source of the slow solar wind (Borrini *et al.*, 1981; Feldman *et al.*, 1981; Gosling *et al.*, 1981).

The slow solar wind formation mechanism is still unclear. It has long been believed that the slow wind in the streamer belt is formed due to the plasma motion from the solar surface along open magnetic tubes that are adjacent to the bases of the streamers at their flanks (see, for example, Wang and Sheeley, 1990). Alternative mechanisms for slow wind formation have also been discussed recently. Uchida *et al.* (1992) suggested that the slow wind is produced as a result of a destabilization of coronal loops. Bochsler *et al.* (1994) argued that the slow wind can be produced by upward traveling plasmoids. Sheeley *et al.* (1997) suggested that the slow wind in the streamer belt is formed due to a continuous generation – from the cusp region of the coronal streamer (as a consequence of magnetic reconnection processes) – of plasmoids, 'blobs'. Finally, Noci *et al.* (1997) suggested a model, according to which the slow wind is formed starting from the solar surface inside the helmet bases of coronal streamers, and represents the plasma motion along open magnetic field lines between neighboring portions with closed field lines. When constructing their model, Noci *et al.* (1997) relied on their studies of coronal

Solar Physics **200:** 259–281, 2001.

streamers using UVCS/SOHO, and results derived from analyzing the content (in coronal streamers) of heavy ions with large first ionization potential.

With the white-light corona data from the LASCO-SOHO instrument becoming available, considerable progress has been made in the study of the slow wind properties in the streamer belt within distances $R > 3R_0$ (here R_0 is the solar radius). Thus, Eselevich and Elselevich (1999, henceforth referred to as Paper 1) showed that at minimum solar activity within distances $R > 3R_0$ in the absence of coronal mass ejections (CMEs), the streamer belt represents a sequence of radial rays of increased brightness. A minimum angular size of a separate ray $d \sim 2–3$ deg. The lifetime of the most long-lived rays can be as long as 10 days. It was also established that these rays are formed by anti-sunward traveling plasma. Furthermore, the rays seem to support both quasi-stationary plasma flows (quasi-stationary solar wind (SW)) whose parameters vary relatively slowly, with the typical time equal to the ray's lifetime (Paper 1; Eselevich and Eselevich, 2000), and sporadic (non-stationary) plasma motions with a typical time of variation of parameters of several hours. The quasi-stationary solar wind velocity in the rays of the streamer belt increases gradually with the distance from the Sun, and reaches $V > 170$ km s^{-1} at $R \approx 15\ R_0$ (Eselevich and Eselevich, 2000), which corresponds to the slow wind velocities expected within these distances. It is conceivable that a slow wind, yet of a somewhat smaller density, also flows between the rays where the corona's brightness is decreased, and relevant measurements are difficult.

Sporadic plasma flows (in the absence of CMEs) in the streamer belt also includes (a) anti-sunward traveling inhomogeneities of material, called the 'blobs', which are produced in a random fashion in separate rays (Sheeley *et al.*, 1997; Wang *et al.*, 1998); and (b) the recently discovered sporadic plasma flows, directed both anti-sunward and sunward, which arise at the time of decay of the streamer, probably as a consequence of the process of magnetic field line reconnection (Wang *et al.*, 1999a, b). A non-stationary SW should also include the occasionally observed formation stage of a quasi-stationary SW when the anti-sunward traveling plasma occupies the ray (Eselevich and Eselevich, 2000).

A fundamental problem in solar wind research involves identifying long-lived rays in which essentially a quasi-stationary SW flows, and determining SW characteristics in them from white-light corona observations. Specifically these characteristics include the electron density (about equal to the plasma density) $n(R)$ in a traveling plasma. Different data and methods are used to determine the plasma density $n(R)$ in the corona: photometric and polarimetric observations of the corona during solar eclipses, observations using K-coronagraphs, radio observations of the corona, and radio probing of the corona using natural radio sources and emitters on-board spacecraft (see reviews by Gulyaev, 1984; Schwenn and Marsch, 1990; Koutchmy, 1997). In these efforts, based on data obtained during eclipses and using most of the K-coronagraphs it is possible to determine the electron density distribution to within distances usually not exceeding 6 R_0 (R_0 being the solar radius).

On the other hand, the distribution of $n(R)$ along a particular coronal ray has not yet been possible to obtain by radio probing the corona.

Despite a large body of existing solar eclipse observations, radial distributions of the plasma density $n(R)$ in separate rays of the streamer belt were obtained for a relatively small number of events (Dollfus and Martres, 1977; Koutchmy, 1997). Furthermore, it is still unclear, to what extent they reflect the plasma density distributions of a quasi-stationary SW and how large the contribution from a non-stationary (sporadic) SW is in these measurements. It remains also to be seen how much the measured distributions of $n(R)$ correspond in each particular case to a single given ray over the length of the entire measured portion along the radius.

The objective of this paper is: for the minimum solar activity and the start of its enhancement (a) to discriminate the rays of the streamer belt with quasi-stationary and non-stationary SW flows; (b) to study the radial distributions of plasma density and velocity in rays with a quasi-stationary SW within $R > 4\ R_0$.

2. Data

The investigations were made using the brightness data on the white-light corona from the LASCO C2 and C3 instruments on-board the SOHO spacecraft which were available via the Internet. Coronagraphs C2 and C3 provide white-light corona images within $R = 2–6\ R_0$ and $R = 3.7–30\ R_0$, respectively. Daily images in the MPEG format were used. The time between images averaged ~ 1 h.

The analysis was based on using selected data for the years 1996 and 1997, corresponding to minimum solar activity and the start of its enhancement, respectively.

To minimize the possible influence of the characteristics of the data analyzed, we adhered to the following approaches:

(1) Only sufficiently bright ray structures (whose brightness exceeded markedly the ambient background brightness) within distances from the solar center $R \sim 2–20\ R_0$ were investigated.

(2) Relative variations of the spatial distributions of coronal brightness rather than their absolute values were studied. The time interval in each case involved did not exceed ten days. This permitted us to eliminate the influence of the possible gradual variations in the instrument characteristics with time.

(3) We studied the radial structures in the corona for which the projection Λ of the latitude onto the plane of the sky (apparent latitude) did not exceed $\pm 30°$. The count of Λ is positive northward of the equator and negative southward.

3. Identifying the Rays in the Streamer Belt – Method of Analysis

A narrow ray ($d \approx 2$–3 deg) of the streamer belt is easy to identify visually in corona images in the coronagraph's field of view whenever it lies in the portion of the streamer belt elongated along the meridian (Paper 1). The possibility of identifying and following, during a reasonably long time interval, individual rays in other portions of the streamer belt is associated with the remarkable property of images of such rays in the plane of the sky, namely, the apparent latitude of the ray Λ in the plane of the sky (the angle between the visible image of the ray in the plane of the sky and the equatorial plane) varies with a change of the position of the ray with respect to the plane of the sky (longitude of the ray) with solar rotation (Hundhausen, 1993). The character of this variation depends on the actual latitude of the ray λ on the Sun (i.e., on the angle between the ray and the equatorial plane) and the heliographic latitude of the Sun's center B_0. As a result, the ray on the synoptic map will describe a certain curve (normally an arc whose convexity is directed equator ward), the equation for which (in the latitude – Carrington longitude coordinates), depending on λ for a particular case $B_0 = 0$ and $B_0 \neq 0$, respectively, was obtained by Hundhausen (1993) and in Paper 1. This effect, when $\lambda \neq 0$, leads at each instant of time to a separation of neighboring rays lying within the portion of the streamer belt extended along the parallel, i.e., they are at different angular displacements from the plane of the sky and hence have a different apparent latitude Λ. As is revealed by a visual examination of the synoptic maps of coronal brightness distributions based on the LASCO data, which are available via the Internet, this procedure identifies most clearly the rays lying at the top of the bend of the streamer belt at a maximum distance to the north or south from the solar equator (Eselevich and Eselevich, 2000). It is such rays, along with those forming the portion of the streamer belt along the meridian, which were used in our analysis.

The procedure of deriving experimental information from images of the light-white corona involved the following steps.

For each image obtained from daily MPEG files, we constructed (depending on the problem to be solved) the brightness distributions $P(\Lambda)$ of the corona at different fixed distances R from the solar center, separately for E or W limb or $P(R)$ for different fixed Λ. We investigated the dynamics of the $P(\Lambda)$ and $P(R)$ distributions with the time t or, equivalently – depending on the angle Ψ_L of deviation of the ray from the plane of the sky. In this case the angular scale $\Psi_L \approx 13.2^\circ$ corresponded to the time scale $t = 24$ h. As the quantity P_J, characterizing the excess of the ray brightness over the surrounding plasma, we used the quantity $P_J = P_M - P_B$, where P_M is a maximum brightness of the ray, and P_B is an arbitrary brightness level of background plasma represented by the smallest minimum in the distribution of $P(\Lambda)$ at a fixed R (see Figure 1 where the values of P_M are presented for rays 2 and 4). Assuming that the elevated brightness of the rays of the streamer belt compared to background plasma is caused mainly by the

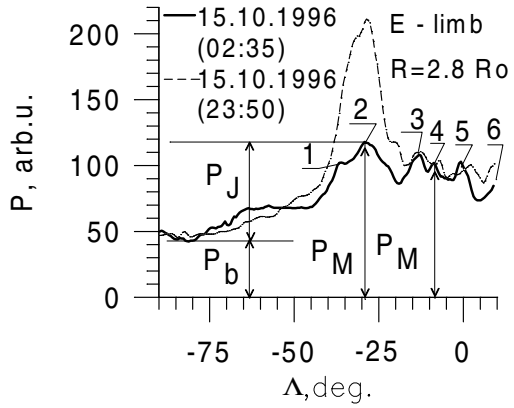

Figure 1. Profiles of the white-light corona brightness distributions P versus latitude Λ in the plane of the sky for the portion of the streamer belt extended along the meridian, 15 October 1996, for two consecutive times: 02:35 UT (*solid line*), and 23:50 UT (*dashed line*). The count of Λ is positive to the north of the equator. Data from LASCO C2, E limb, $R = 2.8\ R_0$.

contribution of the K-corona, we have: $P_J/P_0 = n_J/n_0$, where $P_J = P_0$ and $n_J = n_0$ at $\Psi_L = 0$, i.e., when the ray position coincides with the plane of the sky. (Note that a different choice of an arbitrary level of P_B affects all results obtained below only slightly.) Next, the resulting relative distributions of P_J/P_0 and P_R/P_0 were compared with calculated ones.

4. Criteria for SW Flow Quasi-Stationarity in an Individual Ray of the Streamer Belt

The most general conclusion which is readily apparent from an analysis of the LASCO data is that the brightness at any fixed point of the plane of the sky in any particular structure of the corona (including any particular ray of the streamer belt) is time variant. Such variations are caused principally by solar rotation and unsteady-state processes in the coronal structures under investigation. As a consequence of solar rotation, the selected element decreases in brightness with its distance from the plane of the sky and, accordingly, increases in brightness as it approaches the plane of the sky (Hundhausen, 1993). As will be shown below, the typical scale of such variation is about two or three days. Against this background it is quite easy to distinguish relatively fast non-steady-state changes in brightness with a scale of a few hours or shorter (such as 'blobs' and CMEs) (Sheeley *et al.*, 1997; Paper 1). At the same time separating slower non-stationary changes in brightness (with a scale of $\sim$ 24 h or longer) and quasi-stationary changes when time variations in brightness are due to solar rotation only, involves some difficulties. It turns out that in some cases such a separation is feasible, based on the character of the distributions of $P_J(R)/P_0$ and their time variations, as well as

on the character of the measured dependencies $P_J(\Psi_L)/P_0$ (or equivalent dependencies $P_J(t)/P_0$). Below are formulated the criteria for the fact that the measured distributions of $P_J(R)/P_0$ and $P_J(\Psi_L)/P_0$ for a particular ray in the streamer belt are quasi-stationary, i.e., their time variations over the course of several days are due mainly to solar rotation. Before doing this, however, we wish to emphasize the following two points:

(1) Nowadays there are a limited number of observations of the corona (about ten) made during solar eclipses where plasma density distributions $n(R)$ were measured in individual rays of the streamer belt (see, for example, Dollfus and Martres, 1977). These observations suggest that for $4\ R_0 \leq R \leq 6\ R_0$ the radial distributions of $n(R)$ are reasonably well approximated by the relationship $n \sim R^{-\alpha}$ where the value of $\alpha = \alpha_1$, average for this distance, can vary from 3 to 5 in different rays. On the other hand, direct plasma density measurements in interplanetary space within $64\ R_0 < R \leq 215\ R_0$ showed that $n(R)$ here can also be approximated by an exponential dependence with an average (over this distance) value of $\alpha = \alpha_2 \approx 2.2$ (Schwenn and Marsch, 1990). Correspondingly, within the distances $6\ R_0 \leq R \leq 64\ R_0$ the $n(R)$-distribution is also representable by the relationship $n \sim R^{-\alpha}$ with the exponent α that varies smoothly from the values of α_1 at $R = 6\ R_0$ to the value of α_2 at $R = 64\ R_0$.

(2) The radial distributions of relative brightness $(P_J(R)/P_0)_m$ measured in the ray at fixed times, because of the presence of a neutral radial filter in the LASCO instrument, do not coincide with true distributions of relative white-light corona brightness along the ray $P_J(R)/P_0 = n_J(R)/n_0$.

Taking into account these factors, and also for the lack of information about the characteristics of the radial filter of the LASCO coronagraph, when selecting the quasi-stationarity criterion for brightness ray structures of the streamer belt, the problem facing us was to determine, from $(P_J(R)/P_0)_m$ measurements, the true distributions of $n_J(R)/n_0$. To solve this problem we suggested a new method substantiated in the Appendix to this paper (see also the next section of this paper). The ideology of the method implied that a radial distribution of relative plasma density along a narrow ray can be obtained from the time dependence (or Ψ_L) of relative brightness $P_J(t)/P_0 = P_J(\Psi_L)/P_0$ of such a ray when the brightness is measured along the line of sight normal to the plane of the sky and lying at a fixed distance R_B from the solar center (see Figure 11 in the Appendix). In this case the radial dependencies $n_J(R)/n_0$ are determined for distances $R > R_B$ (see Figure 11 and formula (4) in the Appendix). That the radial filter has no influence on the distribution of $n_J(R)/n_0$ is obvious in this case, because for all R the filter transmission is identical at a fixed distance R_B. All $P_M(R)$ (or $P_J(R)$) start from $R = 4\ R_0$, because at $R \leq 4\ R_0$ many images of the corona used in our analysis were over-saturated in brightness. Essentially, the method is as follows. The distributions of relative brightness in the ray $P_J(t)/P_0 = P_J(\Psi_L)/P_0$ measured at $R_B = 4\ R_0$ during several days are used to estimate plasma densities n_E at the Earth's orbit (for details see the next sections of the paper). If the values of n_E,

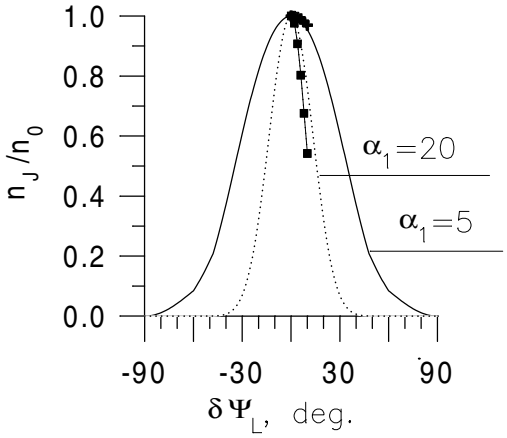

Figure 2. Profiles of the measured normalized variation in density $n_J/n_0 = P_J/P_0$ versus angular deviation Ψ_L from the plane of sky for isolated rays 4 (*crosses*) and 2 (*boxes*) in the event of 15 October 1996 (in Figure 1), E limb, $R = 2.8\ R_0$. *Solid* and *dotted curves* – calculation of the relative brightness $P_J(\Psi_L)/P_0$, respectively, for $\alpha_1 = 5$, $\alpha_1 = 20$, and $\alpha_2 = 2.2$.

thus determined, are within the measured values $\sim$ 10–50 cm^{-3}, then the SW flow in the ray (or the distribution of $n_J(R)/n_0$) is considered quasi-stationary. If there is $n_E < 0.5$ cm^{-3} determined in this manner, then plasma flow in the ray is non-stationary. For the intermediate values $0.5 < n_E < 10$ cm^{-3} (see Section 6 of this paper) further investigation is needed, in view of the possible error of estimating n_E by the method described above. To illustrate the effectiveness of this method we determine the character of the plasma flow in two arbitrary rays of the streamer belt in which an analysis of the distributions of $P_J(t)/P_0 = P_J(\Psi_L)/P_0$ measured at $R_B = 4\ R_0$ led to the following density distributions. In ray A: within $4\ R_0 < R < 6\ R_0$ the relative densities $n(R)/n_0 \sim R^{-\alpha}$, where $\alpha = \alpha_1 = 5$ (this corresponds to the fastest measured decline in electron density in this portion of the corona (Dollfus and Martres, 1977); within $12\ R_0 < R < 215\ R_0$ it will also be assumed that $n(R)/n_0 \sim R^{-\alpha}$, where $\alpha = \alpha_2 = 2.2$ (see Section 6 of this paper), and within $6\ R_0 < R < 12\ R_0$ with $\alpha = (\alpha_1 + \alpha_2)/2 = 3.6$; in ray B: $\alpha_1 = 20$, the intermediate value of $\alpha = (\alpha_1 + \alpha_2)/2 = 11.1$, and $\alpha_2 = 2.2$. With the largest plasma density $n \approx 5 \times 10^6$ cm^{-3} measured in the coronal ray at $R = 4\ R_0$ (Dollfus and Martres, 1977), we have in this case for ray A the value of $n_E \approx 50$ cm^{-3}, which is consistent with observations; for ray B we have $n_E \approx 10^{-5}$ cm^{-3}, which is several orders of magnitude less than the measured values of plasma density in a slow SW at the Earth's orbit. (When $3 < \alpha_1 < 5$, for $n(R = 6\ R_0) \approx 5 \times 10^6$ cm^{-3} the estimated values of n_E lie in the range 10 cm^{-3} $< n_E <$ 50 cm^{-3}, which is also consistent with observations). Figure 2 shows the calculated (in accordance with formula (4) in the Appendix) distributions of relative brightness $P_J(\Psi_L)/P_0$ for rays A (solid line) and B (dashed line).

Thus $n(R)$-distributions with $\alpha_1 = 20$ cannot exist in quasi-stationary slow SW streams in rays of the streamer belt. In other words, the SW with a distribution of $n_J(R)/n_0$ which is characterized by $\alpha_1 \geq 20$, is non-stationary. In view of the error with which we can determine the value of n_E using the procedure described above, such SW flows can be assigned with confidence to non-stationary SW flows, for which a calculation of n_E gives the values of $n_E < 5 \times 10^{-1}$ cm^{-3}, which corresponds to $\alpha_1 > 8$. At the values $5 < \alpha_1 < 8$, further investigation is needed for determining whether SW flow in the ray is quasi-stationary or non-stationary.

Another criterion for the manifestation of non-stationarity is the detection of radially directed movement of non-uniformity fronts of different types in the $P(R)$-distribution (Paper 1).

A separation of the rays with a quasi-stationary and non-stationary SW is illustrated in Figure 1. The figure presents the dependence $P(\Lambda)$ for a part of the portion of the streamer belt extended along the meridian on E limb and at $R = 2.8\ R_0$ for two consecutive times: $t_1 =$ 15 October 1996 (02:35 UT) (solid line), and $t_1 =$ 15 October 1996 (23:50 UT) (dashes). It is evident from Figure 1 that six rays are observed over the interval $\Lambda = (-40^\circ) - (+10^\circ)$. On the synoptic map of the magnetic field on the source surface CR 1915 (*Solar Geophysical Data*, N, P. 1. 1996) segment (elongated along the meridian) of the neutral line of 21–22 October 1996 (its date on the synoptic map is determined by adding to t_1 and $t_2 \approx 6$ days). According to Paper 1, the neutral line passes through brightness maxima of these rays. Since rays 2 and 4 somewhat increase in brightness in Figure 1 between the time t_1 (solid curve) and the time t_2 (dashed curve), this implies that they approach the plane of the sky. Crosses and boxes in Figure 2 show the observed $n_J/n_0 = P_J/P_0$ profiles, respectively, for rays 2 and 4 at a gradual transition from the time t_1 ($|\Psi_L| \approx 12^\circ$) to t_2 ($\Psi_L \approx 0^\circ$). It is evident from Figure 2 that the SW in ray 4 (as well as in rays 3, 5 and 6) is a quasi-stationary one, because the crosses lie near and above the solid thick curve ($\alpha_1 \leq 5$), and in rays 1 and 2 the SW is a non-stationary one, because the dashed curve with black boxes is steeper than the thin solid curve (i.e., $\alpha_1 \geq 20$).

5. Determining the Radial Quasi-Stationary Distributions of Plasma Density in Separate Rays of the Streamer Belt

Three events were used in the analysis, which clearly exhibit a ray located at the bend point of the belt that is at a maximum distance northward or southward of the solar equator. As has already been pointed out above, each such ray is seen on the synoptic map of the white-light coronal brightness (at a given distance from the Sun) as a segment of a thin white arc, with its convexity usually facing the equator. The rays used in the analysis were not disturbed by a coronal mass ejection (CME) during $\sim$10 days or longer. The agreement between the observed position and form

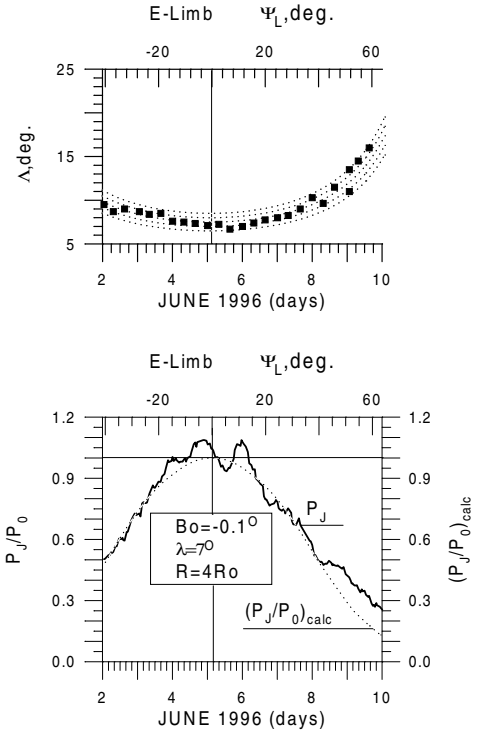

Figure 3. Isolated ray of the streamer belt located at the bend point of the belt at a maximum distance from the solar equator at the northern latitude $\lambda = 7$, at its passage of the plane of the sky at the E limb, on 5 June 1996 (the time is indicated along the lower abscissa axis). *Upper panel*: *solid squares* – dependence of the apparent latitude Λ to the plane of sky of the observed positions of brightness maxima of the rays P_M on the angular deviation Ψ_L of the ray under consideration with respect to the plane of the sky; *dotted lines* – calculated curves, similar to observed ones, for $\lambda = 6.5$, 7.0, 7.5, 8.0, and 8.5°. *Lower panel*: *thick line* – the observed time dependence of the value of the normalized jump of relative brightness P_J/P_0 (relative brightness of the ray); *dotted line* – calculated curve for the values of $\lambda = 7.0°$, $B_0 = -0.1°$, $R = 4\ R_0$, and $\alpha_1 = 3.3$, $\alpha_2 = 2.2$.

of the arc on the synoptic map and the calculated positions makes it possible to reliably identify each individual ray (as shown in Paper 1).

We begin our treatment with two events: 2–9 June 1996, E limb, latitude $\lambda \approx 7.5°$ N, and 14–23 June 1996, W limb, latitude $\lambda \approx 8.5°$ N (it will be recalled that $\Lambda = \lambda$ when $\Psi_L = 0$).

Solid squares in the upper panels of Figure 3 and 4 correspond to experimental locations of brightness maxima of the rays P_M at consecutive times at $R = 4\ R_0$, respectively, for 2–9 June 1996 (E limb), and for 14–23 June 1996 (W limb). The lower abscissa axis indicates the time of observation of the ray at the W or E limb, and the upper abscissa axis indicates the deviation Ψ_L of the ray from the plane of the sky.

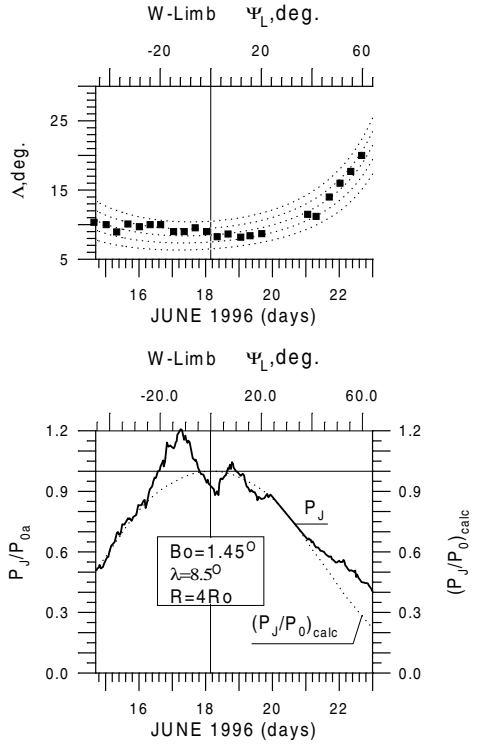

Figure 4. Same as in Figure 3, but for the 2nd isolated ray of the streamer belt: northern latitude $\lambda \approx 8.5°$, passage of the plane of the sky on W limb on 18 June 1996. Calculated curves are given for $\lambda = 6.5, 7.5, 8.5, 9.5$, and $10.5°$, $B_0 = 1.45°$, $R = 4\ R_0$, $\alpha_1 = 3.3$, $\alpha_2 = 2.2$.

The families of the calculated curves $\Lambda(\Psi_L)$ for latitudes λ close to those of the observed rays, respectively, for $B_0 = -0.1°$ (Figure 3) and $B_0 = 1.45°$ (Figure 4) are shown by dotted curves. One can see that the observed curves are in satisfactory agreement with the calculated curves: for $\lambda \approx 7.5°$ (Figure 3, upper panel), and $\lambda \approx 8.5°$ (Figure 4, upper panel). Maximum deviations of the measured values of Λ from the respective calculated values for the ranges of variation of Ψ_L under consideration do not exceed $\pm 0.7°$ in Figure 3, and $\pm 1°$ in Figure 4.

Experimental dependencies of the normalized excess of the brightness of the ray over the surrounding plasma brightness P_J/P_0 on time t (or Ψ_L) for each of these rays at $R_B = 4\ R_0$ are shown in the lower panels of Figures 3 and 4 by full circles. The calculated curves (dotted lines) are obtained for the dependence $n(R)$ that was approximated in each, following each other, portions of length $\delta R \leq R_0$ within distances $R \geq 4\ R_0$ by the relationship $n_0[R/4\ R_0]^{-\alpha} = n_0[1/\cos\ \Psi_L]^{-\alpha}$ (here $R = 4\ R_0/\cos\ \Psi_L$ – see Figure 11 in the Appendix), with smoothly varying values of α from portion to portion. In this case the value of α in each of the sequential portions δR was selected in such a way that the best agreement is obtained between the experimental and calculated curves $P_J(\Psi_L)/P_0$. For $4\ R_0 < R < 6\ R_0$, the

mean value of $\alpha = \alpha_1 \approx 4.2$, and for the calculated curve in the lower panel of Figure 4, $\alpha_1 \approx 3.3$. In Figures 3 and 4, the experimental and calculated curves are shown only for the range of angles $\Psi_L \leq 66°$, which corresponds to the maximum value of $R = R_M \sim 9.8\ R_0$. Experimental distributions of $P_J(\Psi_L)/P_0$ can be constructed with a somewhat smaller accuracy up to the angle of $\sim 80°$, corresponding to a maximum distance of $\sim 21.5\ R_0$. The reason is that for most values of Ψ_L, the identification of the ray along which the distribution of $P_J(\Psi_L)/P_0$ is constructed, becomes less reliable. Since on the E and W limbs the latitudinal arrangement of the ray is virtually identical, $\lambda \approx 7.5°-8.5°$, and its appearance at them is time-shifted by $\sim 13-14$ days (the time of solar rotation by 180°), it is obvious that we are dealing here with the same ray. The distributions of $P_J(\Psi_L)/P_0 = n_J(\Psi_L)/n_0$ for the ray on these limbs are identical, and the variation of α_1 for ~ 14 days is relatively small, ~ 0.9. This corresponds to the rate of time variation in the relative (number) plasma density at the point of the ray at $R = 6\ R_0 \approx 0.033$ part./24 hr, i.e., by 3.3% per day. Hence in this case we are indeed dealing with a quasi-stationary (i.e., varying sufficiently slowly during many days) distribution of $P_J(\Psi_L)/P_0 = n_J(\Psi_L)/n_0$, or a quasi-stationary SW in the selected ray of the streamer belt. Furthermore, the lifetime of the ray exceeds 22 days since the duration of observation of the ray near each limb is ≈ 8 days.

Figure 5 presents one further example of a quasi-stationary distribution of $P_J(\Psi_L)/P_0$ versus time (or Ψ_L) in the selected ray observed during 25–31 August 1996, at the E limb. In this case $\lambda \approx 23°$ N, and $B_0 = 6.9°$. For this event, the distribution of $P_J(\Psi_L)/P_0$ is interpolated by the calculated curve for which α_1 within $4\ R_0 < R < 6\ R_0$ is ~ 4.9, i.e., this distribution is also a quasi-stationary one ($\alpha_1 < 5$). However, it can be observed only on one of the limbs because as the ray moves toward the other limb during ~ 14 days, it is influenced by CMEs and is likely to decay. There may also be other factors that make the investigation of this ray difficult and remain unclear.

Relative distributions of the plasma density n_J/n_0 versus R in separate rays of the streamer belt for the three quasi-stationary distributions of $P_J(\Psi_L)/P_0$ under investigation are presented in Figure 6 in comparison with some of the existing measurements of n_J/n_0 or of the polarized brightness $P_P(\Psi_L)/P_0$ acquired by the *Helios* spacecraft, 1976 ($n_J(R)/n_0$, Esposito, Edenhofer, and Luneburg, 1980), and by the SOHO spacecraft, 1997 ($P_P(R)/P_0$, Romoli *et al.*, 1997). Figure 6 suggests that for a quasi-stationary SW in the rays of the streamer belt the variation of α_1 lies within at least $3 < \alpha_1 \leq 5$, as deduced from a limited amount of data.

To verify the reliability of the results obtained, in the same rays the dependencies $P_J(\Psi_L)/P_0$ were also constructed, and the radial profiles of $n_J(R)/n_0$ were determined for two other distances: $R_B = 5\ R_0$, and $R_B = 6\ R_0$. For $R = 5\ R_0$, the resulting distributions of $n_J(R)/n_0$ within $R \geq 5\ R_0$ are almost coincident with those for $R_B = 4\ R_0$, while for $R_B = 6\ R_0$ the existing differences of the $n_J(R)/n_0$-profiles at $R \geq 6\ R_0$, when compared to the case $R_B = 4\ R_0$, are within

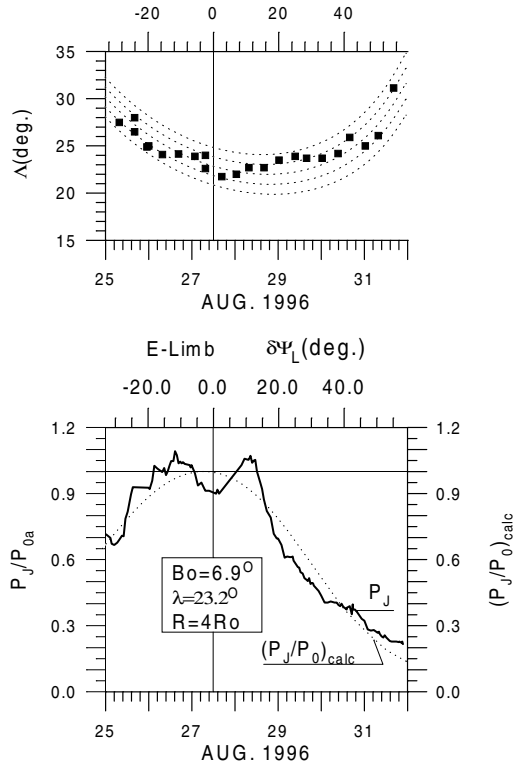

Figure 5. Same as in Figure 4, but for the 3rd isolated ray of the streamer belt: $\lambda \approx 23^\circ$, passage of the plane of the sky on E limb on 27 August 1996. Calculated curves are given for $\lambda = 21$, 22, 23, 24, and 25°, $B_0 = 6.9^\circ$, $R = 4\ R_0$, $\alpha_1 = 4.9$, $\alpha_2 = 2.25$.

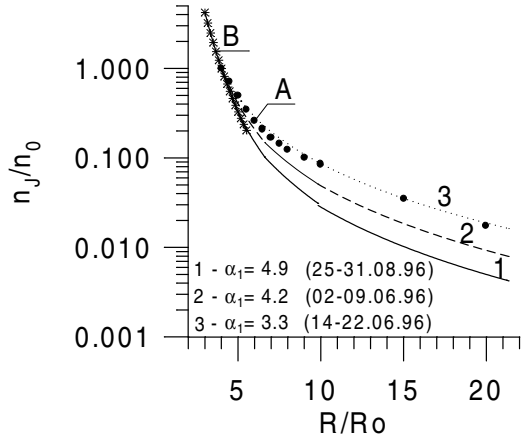

Figure 6. Distributions of the measured normalized density jump $n_J/n_0 = P_J/P_0$ in separate rays of the streamer belt versus R: (A) from the *Helios* data, 1976 (Esposito, Edenhofer, and Luneburg, 1980), (B) according to the data from Romoli *et al.* (1997), (1, 2 and 3) our distributions based on using the LASCO C2 data, respectively, for the events of 25–31 August 1996 ($\alpha_1 = 4.9$); 2–9 June 1996 ($\alpha_1 = 4.2$); and 14–22 June 1996 ($\alpha_1 = 3.3$).

the error of constructing such files. For instance, the mean value of α between $6\ R_0 < R < 8\ R_0$ differs for two distributions of $n_J(R)/n_0$ by 7% at most.

6. A Study of the Velocity Dependencies *V(R)* of a Slow Quasi-Stationary SW in Separate Rays of the Streamer Belt

We investigate the velocity dependencies $V(R)$ of a slow quasi-stationary SW in separate rays of the streamer belt, from $R \approx 4\ R_0$ to the Earth's orbit. In doing so, we take advantage of the law of conservation of mass flow in the rays, $J = n(R)VR^2 = \text{constant}$, the $n(R)$-profiles determined above, the values of n_E and V_E at the Earth's orbit, as well as of the $V(R)$ measured by different methods in separate rays to within $\sim 15\ R_0$. However, first we consider the manifestations, at the Earth's orbit ($R = 215\ R_0$), of the individual rays of the streamer belt, and the SW properties in such rays.

For this purpose, we use the portions of the coronal streamer belt over 20–30 deg in extent (or with a time duration of more than 2 days at a fixed longitude) which are approximately parallel to the solar equator, and depart only slightly (within a few degrees) from the ecliptic plane. As the indicator of the coronal streamer belt, we use the neutral line (NL) of the field on the source surface ($R = 2.5\ R_0$) obtained from calculations of the magnetic field in the corona (Hoeksema and Scherrer, 1986) which at minimum activity satisfactorily coincides with the coronal streamer belt, passing through brightness maxima along the streamer belt (Wilcox and Hundhausen, 1983). This is a so-called 'horizontal' portion of the streamer belt (of the neutral line). In interplanetary space such a portion of the streamer belt corresponds to the region of a slow wind that is extended along longitude and is relatively narrow in latitude (hereinafter referred to as the 'horizontal' heliospheric plasma sheet, HPS), and the neutral line on the source surface corresponds to the heliospheric current sheet (HCS) embedded inside the HPS (the HCS thickness is much less than the HPS thickness) (Eselevich and Fainshtein, 1991; Fainshtein, 1991). When the SW of such a portion reaches $R = 215\ R_0$, the Earth throughout the angular size of this portion $\Delta\Psi_L$ finds itself inside the HPS (and accordingly near the HCS). Thus for several days (several tens of degrees in longitude) the Earth travels virtually along the plasma density maxima in a slow wind near the 'horizontal' portion of the HCS.

Unlike the slow SW region in the neighborhood of the 'tilted' portion of the HCS whose parameters along the path from the Sun to the Earth are distorted due to the solar rotation-induced interaction with a fast SW from coronal holes, the 'horizontal' portions of a slow wind are virtually free from such distortions (Eselevich and Fainshtein, 1991; Fainshtein, 1991). An example of such an event is shown in Figure 7. As is evident from the upper panel of Figure 7, the horizontal segment of the NL (thick solid line) passes through the central meridian of the Sun during 12–15 August 1976 (UT), and lies almost entirely in the ecliptic plane

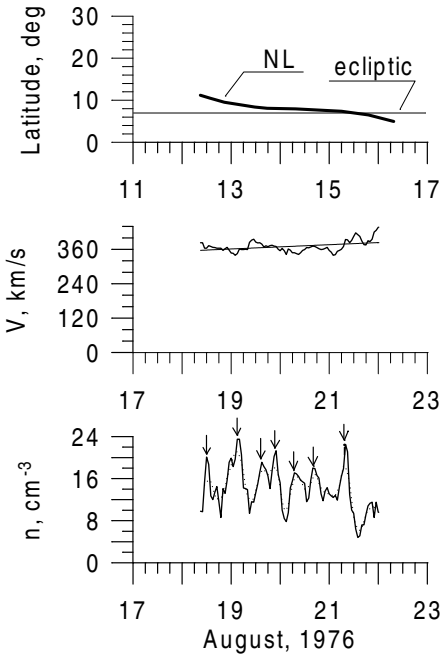

Figure 7. Time dependencies: *top* – the position of the calculated neutral line at $R = 2.5\ R_0$ from Hoeksema and Scherrer (1986) in the 'horizontal' portion of the streamer belt (*heavy solid line*); *thin solid line* – ecliptic line on the source surface; *middle* and *bottom* - solar wind proton velocities and densities (King, 1983) in the 'horizontal' portion of a slow SW in the neighborhood of the HCS at the Earth's orbit.

(thin horizontal line). We determine the dates corresponding to the arrival of this segment of the NL at the Earth's orbit by adding $\Delta t \approx 6$ days to the dates in the upper panel of Figure 7. The value of $\Delta t \approx 6$ days is a typical transit time of a slow SW from $R = 2.5\ R_0$ to the Earth's orbit ($R = 215\ R_0$). This value is obtained in particular by integrating the function $1/V(R)$ over R from $R = 2.5\ R_0$ (the position of the source surface) to $R = 215\ R_0$, where $V(R)$ is the experimental curve in Figure 9 (designated by different symbols). Note also that the distance $R = 2.5\ R_0$ is an approximate distance from the solar center to the 'helmet' top of the streamer.

Thus the portion of the SW from 18–21 August 1976 at the Earth's orbit (middle and lower panels of Figure 7) corresponds to the segment of the NL from 12–15 August 1996 near the solar surface (upper panel of Figure 7). In addition to examining this event, we investigated another six portions of the 'horizontal' heliospheric plasma sheet which were recorded at the Earth's orbit during the following time intervals: 10–15 July 1976; 10–17 September 1976; 8–12 October 1976; 22–3 December 1976; 8–11 May 1977; and 26 September – 8 October 1977. For all of them the $n(t)$- and $V(t)$-dependencies showed the following com-

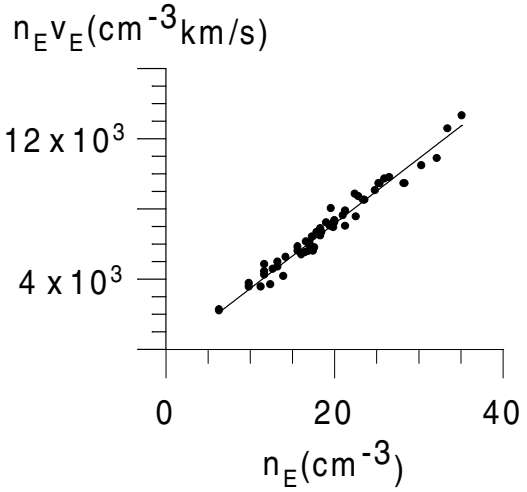

Figure 8. Dependence of the particle flux density j_E at points of maximum values of plasma density n_E in horizontal portions of a slow SW in the neighborhood of the HCS at the Earth's orbit on the value of n_E according to King (1983).

mon characteristic features which are clearly seen in the example of the event in Figure 7.

(1) The oscillation-averaged dependence with a typical period of less than 2° (less than 4 h) – dashed curve in the lower panel of Figure 7 – presents sequences of peaks of 2–3-fold increases in plasma density n_E with a typical angular size of each individual peak of 3–5 deg. Both the relative amplitude and the angular size of these peaks coincide with those of rays with increased brightness in the streamer belt in the Sun's corona (for the examples of such rays see Figure 1). In Figure 7 (lower panel), density maxima corresponding to such rays are shown by the arrows.

(2) The slow solar wind velocity V_E in the neighborhood of the 'horizontal' portions of the HCS varies only slightly. Its value, averaged over seven 'horizontal' portions in the vicinity of the HCS (for which 55 SW plasma density maxima were recorded), was $V_E = 360 \pm 30$ km s^{-1}.

(3) The values of the proton flux density $j_E = n_E V_E$ at $R = 215\ R_0$ in particle density maxima on the 'horizontal' portions of a slow SW can differ nearly by a factor of 4.5, from $j_E \approx 3 \times 10^8$ cm^{-2} s^{-1} to $j_E \approx 1.4 \times 10^9$ cm^{-2} s^{-1}. Furthermore, the variations of j_E are almost linearly related to those in proton density n_E at points of their maxima (Figure 8). This differs fundamentally from the situation in a fast SW stream for which $j_E \approx (2-4) \times 10^8$ cm^{-2} s^{-1}, i.e., it changes little (Feldman *et al.*, 1977; Schwenn and Marsch, 1990), and the value of V_E can vary almost twice for different events ($V_E \sim 400$–800 km s^{-1} is a maximum velocity of a fast SW stream).

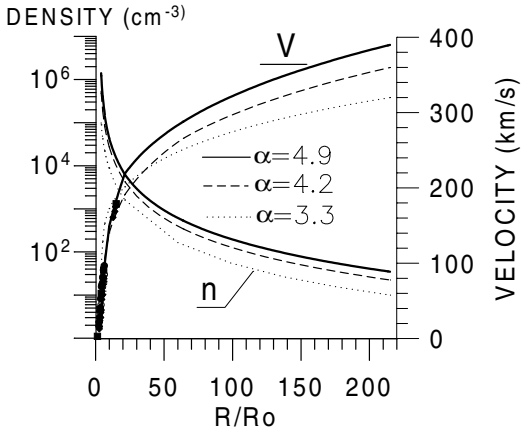

Figure 9. Distributions of the velocity V and density n versus R/R_0 of a quasi-stationary SW flowing in ray structures of the streamer belt and of its extension into interplanetary space, a slow solar wind in the vicinity of the HCS, calculated at different values of α_1, n_E, and V_E: *heavy solid line* – $\alpha_1 = 4.9, n_E = 35$ cm^{-3}, $V_E = 390$ km s^{-1}; *dashed line* – $\alpha_1 = 4.2, n_E = 22.5$ cm^{-3}, $V_E = 360$ km s^{-1}; *dotted line* – $\alpha_1 = 3.3, n_E = 10$ cm^{-3}, $V_E = 330$ km s^{-1}. The different symbols – our measurements of V using three different methods. (Compare Figure 10.)

The data from *Helios 1* and *2* (Schwenn and Marsch, 1990) can be advantageously used to determine the value of V for a slow SW in the vicinity of the HCS at $R \sim 64\ R_0$. It was found to be $V \sim 275 \pm 25$ km s^{-1}.

Within 4–15 R_0, the velocity of a quasi-stationary slow SW in individual rays of the streamer belt was measured by three independent methods (Eselevich and Eselevich, 2000), and the respective results are shown in Figure 10 by different symbols (solid circle; open circle; solid square) – for the movement of the leading edge of SW stream occupying the ray of increased brightness; (open triangle; open square; asterisk) – for the movement of the plasma brightness inhomogeneity (density) carried away by the main SW; and (+) – from the initial velocity of 'blobs'. These measurements which were made for different rays of the streamer belt and for different times in the years 1996–1998 gave $V(R)$-curves with similar profiles. All the above suggests that for a slow quasi-stationary SW the profile of the $V(R)$-curve, all the way from $R \sim 4\ R_0$ to $R \sim 215\ R_0$, varies only slightly in the individual rays of the streamer belt. Furthermore, the mass flow density j and the plasma density n in different rays at any given distance R can differ by more than a factor of 4. This result is consistent with the phenomena (observed in the data from the C2 instrument) of an occasional presence in individual rays of SW plasma streams with different values of j (or n), and with the establishment of quasi-stationary SW flows whose density can differ several times from the pre-existing SW plasma density in the rays before (Eselevich and Eselevich, 2000). This inference is also supported by measurements of absolute values of plasma density n in coronal streamers, showing that the difference of n in separate rays

of the streamer belt within distances as far as $R < 5\ R_0$ can exceed an order of magnitude (Dollfus *et al.*, 1977).

Let us now ascertain how this conclusion agrees with the above measurements of the different values of the index α ($3 < \alpha_1 \leq 5$) in quasi-stationary plasma brightness (density) distributions $P_J(R)/P_0 = n_J(R)/n_0$

To do this, we calculate the dependencies of plasma density $n(R)$ in separate rays of the streamer belt, from $R = 215\ R_0$ to $R = 4\ R_0$, for three typical values of plasma density at the Earth's orbit in 'horizontal' portions of a slow SW: $n_E = 10\ \text{cm}^{-3}$ (minimum), $22.5\ \text{cm}^{-3}$ (medium), and $35\ \text{cm}^{-3}$ (maximum) – see Figure 8. Our calculations will use the relative density distributions obtained earlier to within distances $\sim 10\ R_0$ for three values of α_1: 4.9, 4.2, and 3.3 (Figure 6).

Note that the following procedure of calculating the radial distributions of absolute values of plasma density $n(R)$ in three different rays does not in fact allow us to determine the true density values in the rays under investigation. It is possible to calculate the $n(R)$ in each of the rays considered by using the relative distributions of plasma density obtained above, only based on information about the density values in these rays at a single point at least. No such information is available to us. For that reason, these calculations have an estimating character, and are based on the assumptions that: (a) the resulting characteristics of plasma density drops in separate rays $\alpha_1 = 4.9$, 4.2, and 3.3, are close to the largest, mean and least of the possible values of α_1 in the rays of the streamer belt; (b) the measured values of proton densities at the Earth's orbit in separate rays of the horizontal portion of the streamer belt $n_E = 10\ \text{cm}^{-3}$ (minimum), $22.5\ \text{cm}^{-3}$ (mean), and $35\ \text{cm}^{-3}$ (maximum) are typical of minimum activity; and (c) there is an unambiguous correlation between the above typical values of α_1 and n_E.

It will be assumed that within $R = 64$–$215\ R_0$ the dependence $n(R) \sim R^{-\alpha}$, where the value of α was chosen from the condition that $V(R = 64\ R_0)$, is approximately 12% less than $V(R = 215\ R_0)$ (Schwenn and Marsch, 1990). For the above distances this condition gives the values of $\alpha = 2.2$–2.25 in different rays. The interval $10\ R_0 < R < 64\ R_0$ was divided into 2–3 portions in which α varied from 2.3–2.5 to 2.2–2.25. To perform calculations of $n(R)$ it is also necessary to relate n_E in the ray to the quantity α_1 characterizing the steepness of plasma density decline in the ray within $R = 4$–$6\ R_0$. If it is assumed that a maximum value of $n_E = 10\ \text{cm}^{-3}$ corresponds to a maximum value (of those considered) of $\alpha_1 = 4.9$ at the Earth's orbit, and a maximum value of $n_E = 35\ \text{cm}^{-3}$ corresponds to a minimum value of $\alpha_1 = 3.3$, then from calculations it follows that for the three rays the values of $n(R = 4\ R_0)$ are approximately identical and are equal to a few units per 10^5 particles per cm^3. It seems unlikely that such a result corresponds to actual conditions in the corona. It follows from our analysis of the LASCO data, for example, that within the above-mentioned distances the corona's brightness in different rays at the same values of Ψ_L can vary markedly. Furthermore, measurements of plasma density n during solar eclipses show that in different rays the plasma density $n(R = 4\ R_0)$ can vary over a considerable range

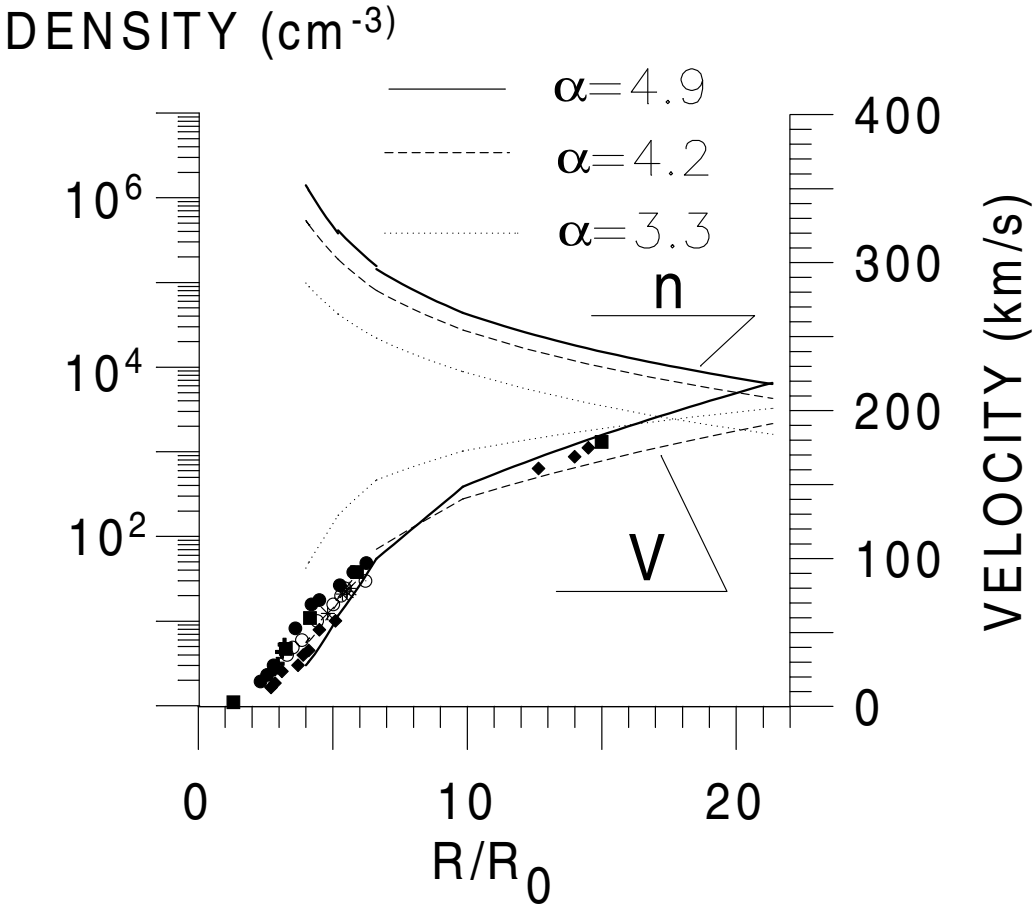

Figure 10. Part of the distributions from Figure 9 near the Sun within 4 $R_0 < R < 22\ R_0$ with higher spatial resolution. The symbols (*solid circle, open circle, solid square*), (*open triangle, open square, asterisk*) and (+) – our measurements of the velocity V using three different methods.

(Dollfus *et al.*, 1977). Therefore, a different variant of correlation of α_1 with n_E was chosen: $\alpha_1 = 4.9$ corresponds to $n_E = 35$ cm^{-3}, the value of $n_E = 22.5$ cm^{-3} corresponds to $\alpha_1 = 4.2$, and $n_E = 10$ cm^{-3} corresponds to $\alpha_1 = 3.3$.

Based on the above considerations, for three rays which in the corona belong to the streamer belt, we constructed the dependencies of plasma densities $n(R)$ in the range of distances $R = 4$–$215\ R_0$ (Figures 9 and 10). As is apparent from Figure 9 and 10, at $R = 4\ R_0$ plasma densities in different rays vary from $\sim 9 \times 10^4$ to 1.4×10^6 cm^{-3}, i.e., they differ more than an order of magnitude, and their values are coincident with those measured earlier which for different observations are $n \sim (10^5$–$2 \times 10^6)$ cm^{-3} (Dollfus *et al.*, 1977; Schwenn and Marsch, 1990; Koutchmy, 1997).

We now turn to the determination of the radial distributions of the slow SW velocity in the rays, based on our obtained $n(R)$-dependencies in Figures 9 and 10. To accomplish this, we make use of the law of conservation of mass flow for each of the rays under consideration: $n(R)V(R)R^2 = n_E V_E R_E^2$, hence $V(R) = n_E V_E R_E^2$ (here the index 'E' refers to the values of parameters at the Earth's orbit). From this relationship it follows that the plasma velocity distribution within the ray depends on the relative (number) density distribution $n(R)/n_E = [n(R)/n(4\ R_0)]n(4\ R_0)/n_E$, and on V_E. As it has been shown above, the distributions of $n(R)/n(4\ R_0)$ can vary in different rays of the streamer belt with a change of α_1, and the slow wind velocity at the Earth's orbit in individual rays can vary in the range of $\sim 360 \pm 30$ km s^{-1} (here $\Delta V_E = \pm 30$ km s^{-1} is the standard deviation of V_E from the mean value 360 km s^{-1} that was determined for 55 rays). In this connection, for determining the radial velocity distributions $V(R)$ it is necessary to ascertain the correspondence between the values of V_E and the distributions of $n(R)/n(4\ R_0)$ (or, equivalently, the values of α_1).This can be done if we relate n_E to V_E for each ray, i.e., a correspondence between n_E and $n(R)/n(4\ R_0)$ (or α_1) in the rays has already been established above. The following correspondence between n_E and V_E seems most realistic: larger values of V_E correspond to larger values of n_E. This is confirmed by, for example, the existence of a positive (yet very weak) correlation between n_E and V_E in density maxima in 'horizontal' portions of a slow wind according to the data from (King, 1983) (we do not give here this dependence for reasons of space). With this taken into account, for the three distributions of $n(R)$ in Figures 9 and 10, the $V(R)$ - dependencies for $V_E = 330$, 360, and 390 km s^{-1} which are also shown in Figures 9 and 10. Furthermore, the SW flow in the ray with the velocities $V_E = 330$ km s^{-1}, $V_E = 360$ km s^{-1} and $V_E = 390$ km s^{-1}, respectively, had the densities $n_E = 10$ cm^{-3}, 22.5 cm^{-3}, and 35 cm^{-3}. At the same time the particle flux density $j_E = n_E V_E$ at such values of n_E and V_E can differ in individual rays nearly by a factor of 4.

It is evident from Figure 10 that the $V(R)$-distributions measured at $R = 4$–15 R_0 give the best fit to the calculated curves at $\alpha_1 = 4$–5, whereas the agreement with calculations is not so good when $\alpha_1 < 4$.

The relatively small (about 4-fold) variation in the profile of the $V(R)$ curve with a change in plasma particle density j_E is a new important characteristic of the slow quasi-stationary SW in rays of the streamer belt. It fundamentally distinguishes the slow wind from the fast SW from coronal holes for which $j_E \approx$ constant for the main part of the fast stream, and there is a plethora of $V(R)$ curves (the value of V_E for different fast streams varies over the range 400–800 km s^{-1}).

7. Conclusions

The main conclusions of this study may be formulated as follows.

(1) We have suggested a method for separating the rays of the streamer belt with quasi-stationary and non-stationary SW flows. It has been shown that the lifetime of rays with a quasi-stationary SW can exceed 20 days.

(2) We have developed a new technique for measuring the relative (number) density distribution of a quasi-stationary slow solar wind (SW) flowing along the increased brightness ray of the streamer belt, based on the LASCO/SOHO data. It has been shown that the law of variation of n for such SW flows has the form $n \sim R^{-\alpha}$, where $\alpha = \alpha_1 \approx 3.3$–$4.9$ within $4\ R_0 \leq R \leq 6\ R_0$, and it decreases gradually with the distance. This is consistent with radial distributions of electron densities in the streamer belt measured by other methods (Dollfus *et al.*, 1977; Esposito, Edenhofer, and Luneburg, 1980; Romoli *et al.*, 1997).

(3) It has been shown that the $V(R)$ profiles in separate rays of the streamer belt differ little from each other, although the value of mass flow density j in them can change more than by a factor of 4. This fundamentally distinguishes the slow SW in rays of the streamer belt from the fast SW from coronal holes, for which $j \approx$ constant, and the dependencies $V(R)$ in different fast streams can differ substantially.

Appendix

The plasma density distribution along a coronal ray can be determined using relationships characterizing the Thompson scattering of photospheric radiation from free electrons of coronal plasma (in the coronal plasma the proportion of admixtures is small and the quasi-neutrality condition is satisfied; therefore, electron density is virtually equal to plasma density or to proton density). For the sake of simplicity, we consider the following idealized model. Let the corona represent a fully-ionized plasma with a spherically-symmetric distribution of electron density $n_B(R)$ – 'background plasma'. A single coronal ray with a relatively small angular size in latitude and longitude, respectively, $\Delta\lambda$ and $\Delta\Psi_L$, is 'embedded' in it. To a first approximation it will be assumed that the ray lies in the solar equatorial plane and the equator coincides with the ecliptic plane. The deviation of the ray from the equatorial plane and the non-coincidence of the equatorial plane and the ecliptic plane will be taken into account later in the text. It will be assumed that electron density in the ray varies with the distance from the solar center as $n_J(R)$, and across the ray it is uniform within the ray width.

As the Sun rotates about its axis, the ray finds itself at different angular differences Ψ_L from the plane of the sky. Just this makes it possible to determine $n_J(R)$ in an isolated ray. This follows from Figure 11, showing the scheme for recording coronal radiation along the line of sight in the case where a separate coronal ray deviates from the plane of the sky by the angle Ψ_L. Indeed, the variation of Ψ_L leads to the fact that the line of sight along which the scattered radiation of the corona is recorded and whose distance from the solar center is R_B crosses the

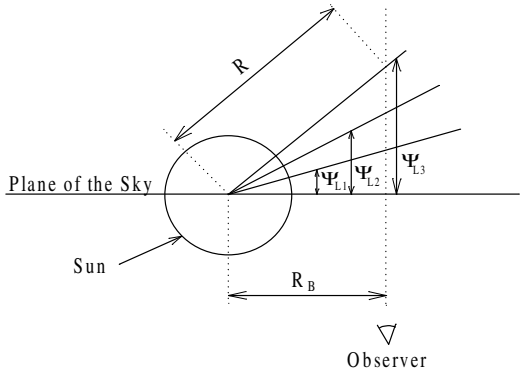

Figure 11. Scheme illustrating the positions of the Sun, the coronal ray in the equatorial plane, and of the line of sight when recording coronal radiation with the coronagraph (view from the north pole of the Sun). Ψ_L – longitude of the ray axis, and R_B is a minimum distance from the solar center to the line of sight.

coronal ray at different distances $R \geq R_B$ which are uniquely related to the angle Ψ_L: $R = R_B/\cos\Psi_L$ Furthermore, by determining the radiation intensity of the ray elements $P_J(R_B, \Psi_L) = P_J(R)$ located at different R, it is possible to find the relative distribution of electron density $n_J(R)$.

To determine $P_J(R)$ we perform calculations similar to those done by Hundhausen (1993). Bearing in mind that we will seek the electron density distribution in the ray starting from $R = 4\ R_0$, we take advantage of the 'point source' approximation used by Hundhausen (1993) ($\sin\Omega = R_0/R \to 0$, where Ω is the angular size of the Sun at the distance R from its center), as well as neglecting the center-to-limb darkening (this can also be done, based on calculations reported by Hundhausen (1993). It will be assumed that for each point along the line of sight the intensity of radiation from each point is composed of two components: P_B and P_J, where P_B is the background plasma radiation intensity. Unlike Hundhausen (1993), it will not be assumed here that electron density in the ray drops with the distance from the Sun exactly in the same fashion as it does in background plasma. For a total coronal radiation intensity along the line of sight we then have:

$$P_M = P_B + P_J = P_B + P^* \int_{\Psi_{L1}}^{\Psi_{L3}} n_J(r)(1 + \sin^2\Psi_L)\,\mathrm{d}x\ , \tag{1}$$

where $P^* = (\pi\sigma/2) I^* {R_0}^2/R$ is the energy flux density of photospheric radiation, and I^* is the Thompson scattering section.

On the other hand, for a narrow ray we have

$$\begin{aligned} P_J &= P^* \int_{\Psi_{L1}}^{\Psi_{L3}} n_J(R_B, \Psi_L)(1 + \sin^2(\Psi_L))\,\mathrm{d}\Psi_L \approx \\ &\approx n_J(R_B, \Psi_L)(1 + \sin^2(\Psi_L)(\Psi_{L3} - \Psi_{L1}) = n_J(1 + \sin^2(\Psi_L))\Delta\Psi\ , \end{aligned} \tag{2}$$

$$P_J = P_M - P_B \ . \tag{3}$$

The quantity

$$P_J(R_B,\Psi_L)/P_0(R_B,0) = n_J(R_B,\Psi_L)(1+\sin^2(\Psi_L))/n_0(R_B,0) \tag{4}$$

can be compared with a corresponding relationship which is determined from the LASCO/SOHO data. By choosing a suitable dependence $n_J(R_B,\Psi_L)$, for which the relationship (4) gives the best fit to that obtained from observations, we can determine the relative (number) density $n_J(R_B,\Psi_L)/n(R_B,0)$ in the ray starting from $R = R_B$. Actually, for different ranges of R we specified a relationship of the form $n \sim 1/R^\alpha$ with a variable α. As a result, in different portions of the angles Ψ_L the expression (4) turned out to be proportional to the relationship

$$P_J \sim P^*(1+\sin^2(\Psi_L))\cos^\alpha(\Psi_L) \ . \tag{5}$$

Let now the ray be at an angle λ to the solar equatorial plane, and let the heliographical latitude of the solar center be B_0. In this case, Equations (1), (2), (4), and (5) must involve, instead of the angle Ψ_L, the angle θ of deviation of the ray from the plane of the sky in the coordinate system XYZ, with its origin at the Sun's center where the axis X is directed earthward, the axis Y lies also in the ecliptic plane, and the axis Z is perpendicular to the ecliptic plane. The angle θ is related to the angle Ψ_L by the relation (Paper 1)

$$\sin(\theta) = X/R = \cos(\lambda)\cos(B_0)\sin(\Psi_L) + \sin(\lambda)\sin(B_0) \ , \tag{6}$$

where X is a coordinate of the point on the ray at the distance R from the origin of coordinates. In this case it was assumed that the coordinate system XYZ and the coordinate system $X'Y'Z'$ that is 'tied' to the solar equator are characterized by the following correlation: the axes Y and Y' are coincident, the axis X is in the plane $X'Z'$, and the axis Z is inclined to the axis Z' by an angle B_0.

Acknowledgements

We are grateful to V. M. Mikhalkovsky for his assistance in preparing the English version of the manuscript. Grant governmental support for Russian Federation's leading scientific schools N961596733 and GNTP 'Astronomy'.

The SOHO/LASCO data used here are produced by a consortium of the Naval Research Laboratory (USA), Max-Planck-Institute für Aeronomie (Germany), Laboratoire d'Astronomie (France), and the University of Birmingham (U.K.). SOHO is a project of international cooperation between ESA and NASA.

References

Bochsler, P.: 1994, *UVCS Experiment Handbook*, p. 72.

Borrini G., J. T. Gosling, S. J., Bame, W. C., and Feldman, J. M.: 1981, *J. Geophys. Res.* **86**, 4565.

Dollfus, A. and Martres, M.-J.: 1977, *Solar Phys.* **53**, 449.

Eselevich, V. G. and Fainshtein V. G.: 1991, *Planetary Space Sci.* **39**, 1123.

Eselevich, V. G. and Eselevich, M. V.: 1999, *Solar Phys.* **188**, 299 (Paper 1).

Eselevich, V. G. and Eselevich, M. V.: 2000, *Solar Phys.* **197**, 101.

Esposito, P. B., Edenhofer, P., and Luneburg E.: 1980, *J. Geophys. Res.* **85**, 3414.

Fainshtein, V. G.: 1991, *Solar Phys.* **136**, 169.

Feldman, W. C., Asbridge J. R., Bame S. J., and Gosling J. T.: 1977, in: O. R. White (ed.), *The Solar Output and Its Variations*, Colorado Associated University Press, Boulder, CO., p. 351.

Feldman W. C., Asbridge J. R., Bame S. J., and Gosling J. T.: 1981, *J. Geophys. Res.* **86**, 5408.

Gosling J. T., Borrini G., Asbridge J. R., Bame W. C., Feldman W. C., and Hansen R. T.: 1981, *J. Geophys. Res.* **86**, 5438.

Gulyaev, R. A.: 1984, *Itogi nauki I tekhniki, seriya Astronomiya*, Vol. 25, VINITI, Moscow, p. 3.

Hoeksema J. T. and P. H. Scherrer: 1986, CSSA ASTRO 8511, World Data Center A for Solar-Terrestrial Physics, Boulder, Rep. UAG-94.

Hundhausen, A. J.: 1993, *J. Geophys. Res.* **98**, 13177.

King, J. H.: 1983, *Interplanetary Medium Data Book - Supplement 2 (1978–1982)*, NASA, USA.

Koutchmy, S.: 1997, in: Z. Mouradian and M. Stavinschi (eds.), *Theoretical and Observational Problems Related to Solar Eclipses*, NATO ASI Series, Series C: Mathematical and Physical Sciences, Vol. 494, Kluwer Academic Publishers, Dordrecht, p. 39.

Noci, G., Kohl, J. L., Antonucci, E., Tondello, G., Huber, M. C. E., Fineschi, S., Gardner, L. D., Korendyke, C. M., Nicolosi, P., Romoli, M., Spadaro, D., Maccari, L., Raymond, J. C., Siegmund, O. H. W., Benna, C., Ciaravella, A., Giordano, S., Michels, J., Modigliani, A., Naletto, G., Panasyuk, A., Pernechele, C., Poletto, G., Smith, P. L., and Strachan, L.: 1997, *Proceedings of the Fifth SOHO Workshop*, 'The Corona and Solar Wind Near Minimum Activity', Oslo, Norway 17–20 June 1997, ESA SP-404, p. 75.

Romoli, M., Biesecer, D., Benna, C., Fineschi, S., Lamy, P. L., Llebaria, A., Kohl, J. L., and Noci, G.: 1997, *The Corona and Solar Wind Near Minimum Activity*, 17–20 June 1997, Oslo, Norway, ESA, SP-404, p. 637.

Sheeley, Jr., N. R., Wang, Y.-M., Hawley, S. H., Brueckner, G. E., Dere, K. P., Howard, R. A., Koomen, M. J., Korendyke, C. M., Michels, D. J., Paswaters, S. E., Socker, D. G., Cyr, O. C. St., Wang, D., Lamy, P. L., Liebaria, A., Schwenn, R., Simnett, G. M., Plunkett, S., and Biesecker, D. A.: 1997, *Astrophys. J.* **485**, 472.

Schwenn, R. and Marsch, E. (eds.): 1990, *Physics of the Inner Heliosphere*, Part 1, *Large-Scale Phenomena*, Series Physics and Chemistry in Space, Space and Solar Physics, Vol. **20**, Springer-Verlag, Berlin.

Uchida, Y., McAllister, A., Strong, K. T., Ogawara, Y., Shimozu, T., Matsumoto, R., and Hudson, H. S.: 1992, *Publ. Astron. Soc. Japan* **44**, L155.

Wang, Y.-M. and Sheeley, N. R., Jr.: 1990, *Astrophys. J.* **355**, 726.

Wang, Y.-M., Sheeley, Jr. N. R., Walters, J. H., Brueckner, G. E., Howard, R. A., Michels, D. J., Lamy, P. L., Schwenn, R., and Simnett, G. M.: 1998, *Astrophys. J* **498**, L165.

Wang, Y.-M., Sheeley, Jr. N. R., Howard, R. A., Cyr, O. C. St., and Simnett, G. M.: 1999a, *Geophys. Res. Lett.* **26**, 1203.

Wang, Y.-M., Sheeley, Jr. N. R., Howard, R. A., Rich, N. B., and Lamy, P. L.: 1999b, *Geophys. Res. Lett.* **26**, 1349.

Wilcox J. M. and Hundhausen, A. J.: 1983, *J. Geophys. Res.* **88**, 8095.